RESEARCH ACTIVITIES III
Department of Electronic Structure

III-A Synthesis and Characterization of Exotic Molecule Based Nano-Crystals of Metal Acetylides: Toward Carbon Encapsulated Metal Dot Array, Metal Nano-Networks and Metal-Carbon Hybrid Devices

Metal-carbon binary junctions are expected to exhibit interesting properties, such as Shottoky barrier rectification, optical and tunneling devices, and chemical protector against oxidation. Metal acetylides have the ionic bond between the metallic cation and the acetylide anion. In the simplest case, divalent metal cations (M^{2+}) form a fcc lattice structure with a C_2^{2-} anion between the two metal cations. The introduction of alkyl or aromatic group into the C_2 unit, producing R–C≡C$^-$, can generate organometallic cluster compounds $((R–C\equiv C^-)_aM^{a+})_n$, ($a$ = 1, 2), some of which can be isolated as a single crystal. These cluster compounds are soluble in organic solvent and provide solid films with nano-scale planarity by spin-coating method. Photoexcitation of metal-acetylides induces charge-neutralization reaction producing carbon-skinned metal particles, or metallic nanowires or nano-sheets covered with organic polymer matrices. This property leads us for application of photo-lithographical pattern generation of metallic circuits or magnetic arrays. On the other hand, the reaction mechanism of the photoreactions of the respective acetylide systems can be highly dependent on the electronic structure of metal atoms. We are also illuminating the mechanism of these reactions.

III-A-1 Electric Conductivity of Self-Assembled Copper Acetylide Nanowires and Nanocables

JUDAI, Ken; NISHIJO, Junichi; NISHI, Nobuyuki

[*Adv. Mater.* in press]

We have found that copper acetylide (C_2Cu_2) molecules self-assemble into ultra thin nanowires in an aqueous solution at room temperature, and annealing of the C_2Cu_2 nanowires converts to metallic copper nanowires encapsulated in carbon outer layers (nanocables). This copper nanocable core is extremely thin, in which only 8 Cu atoms can line up in the diameter. The electric conductivity of such thin wires becomes important for recent progress of electronic devices.

Actually, the current-voltage (*I-V*) measurement of the nanowires and nanocables was carried out by point-contact using an atomic force microscopy (AFM). Figure 1a illustrates a topological image of a C_2Cu_2 nanowire on Au substrate by AFM. The height observed by AFM was 5 ~ 6 nm, which corresponds to the diameter of a single C_2Cu_2 nanowire. By using a conductive cantilever, *I-V* properties could be observed with point-contacting through the nanowire. Figure 1b shows *I-V* characteristics of contacting onto the nanowire, and the nanocable after the annealing. Without nanowires and nanocables, the direct contact of the cantilever on the substrate showed a normal ohmic *I-V* property. As the cantilever was in contact with the nanowire, non-ohmic behavior was observed in *I-V* measurement. The band-gap of 0.5 ~ 1.5 eV was typically observed as the threshold voltages of the drastic increasing current.

When *I-V* characteristics of the converted nanocables was measured, much larger plateau of no current region was observed to be typically more than ~3 V. This indicates that the nanocable exhibits insulating character through the point-contact by AFM. Annealing of the semiconductive C_2Cu_2 nanowires produced Cu nanowires covered with carbon outer layers. The AFM cantilever was contacting to this carbon outer layers. The measurement by AFM proves that the nanocable is coated with microscopic insulator.

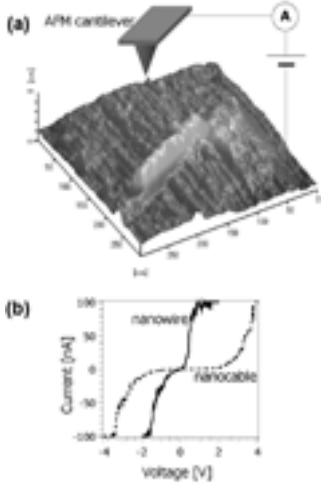

Figure 1. Electric conductive properties of C_2Cu_2 nanowires. (a) AFM image of a C_2Cu_2 nanowire on Au substrate. Schematic diagram is also supplemented for current-voltage (*I-V*) measurement. With using conductive cantilever (Au coated), current between the substrate and the cantilever through nanowires was measured. (b) *I-V* properties of nanowires and nanocables. Although the Au substrate showed ohmic *I-V* character, the C_2Cu_2 nanowire exhibited a non-ohmic property with a small band-gap (solid line). The converted Cu-nanocables covered with carbon provided insulating nature (dashed line).

III-A-2 Crystal Structure of C_2Cu_2 Nanowires by X-Ray Diffraction and DFT Calculation

JUDAI, Ken; NISHI, Nobuyuki

Copper acetylide (C_2Cu_2) molecules self-assembly into nanowires. The X-ray diffraction (XRD) measurement was performed to reveal stacking of C_2Cu_2 molecules in the nanowire. The sample of C_2Cu_2 nanowires exhibited several well-resolved peaks (Figure 1a). Peak widths of XRD measurement can be related to crystalline size by the Scherrer equation. Broader XRD peaks indicate smaller size. The coexistence of the sharp and broad signals for the crystals implies non-spherical crystalline structure of C_2Cu_2.

The density functional theory (DFT) calculation was carried out to assign the XRD spectrum. Various crystal structures have been reported for alkali metal acetylide compounds. We have optimized C_2Cu_2 crystal structure from these reported structures as initial geometries. The obtained structure with the lowest energy is illustrated in Figure 1c, which is essentially the same as the structure of C_2Li_2. The unit cell is orthorhombic (*Immm* No.71, Z = 2) with cell parameters of a = 3.39 Å, b = 4.58 Å, and c = 5.57 Å.

From the optimized crystal structure of C_2Cu_2, XRD spectrum can be simulated. Peak intensity can be calculated from the Lorenz-Polarization factors and the structure factors using DFT optimized unit cell. Peak width can be estimated by the Scherrer equation depending on the size of crystal. When a needle-like crystal (a = c = 5 nm, b = 40 nm) was assumed for their peak broadness, the dominant peaks of the observed XRD spectrum could be reproduced by the simulation (Figure 1b). This simulation suggests that the driving force of self-assembling nanowire production is originated in the highly anisotropic character of the C_2 unit. The b-axis of C_2Cu_2 crystal is the direction of the C_2 unit. The line width in the observed spectrum suggests that the crystal grows along b-axis more rapidly than the other axes.

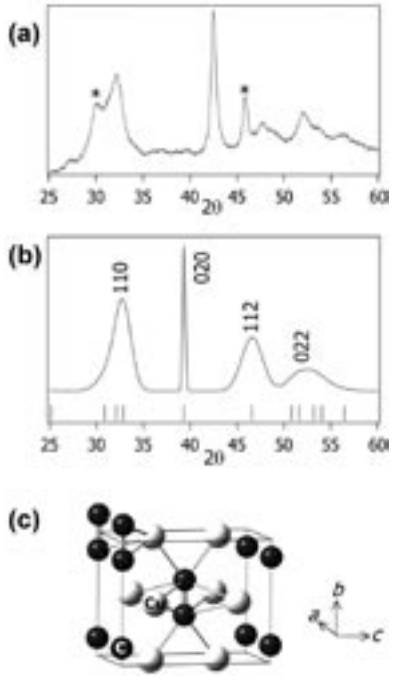

Figure 1. Crystal structure of C_2Cu_2 nanowires. (a) Powder XRD spectrum of C_2Cu_2 nanowires. The XRD results were acquired with X-ray of a Cu Kα line (0.154 nm). (b) Simulated XRD spectrum from the DFT calculated structure. The peak widths were estimated by the Scherrer equation with assumption of a needle shape (a = c = 5 nm, b = 40 nm). The dominant peaks of experimental XRD can be reproduced in the simulation, however, there are still unidentified peaks (labeled with *) of another crystal form. (c) DFT optimized structure of C_2Cu_2. The unit cell is orthorhombic and has body centered symmetry. C_2 units are coordinated with 4 Cu atoms in end-on sites and with 4 Cu atoms in side-on.

III-A-3 Photoconversion of Organometallic Cluster Thin Films to Metallic Copper-Sheets Sandwiched in Polymers

NISHI, Nobuyuki; NISHIJO, Junichi; JUDAI, Ken; OKABE, Chie; OISHI, Osamu

Generation of hot electrons in nanoparticles can be performed with efficient energy pumping from light harvesting π electron networks of organic matrices. Metallic copper is the best material for electronic conduction because of its low resistivity and enthalpy of fusion. $[Cu–C{\equiv}C–t\mathrm{Bu}]_{24}$ cluster molecules contain the light harvesting unit of ethynyl chromophore and the lowest excited π-d charge transfer triplet state. Photoexcitation of $[Cu–C{\equiv}C–t\mathrm{Bu}]_{24}$ films induces segregation of the crystals into metallic and organic phases and leads to evolve the metallic nanosheets sandwiched by organic polymers. High pressure mercury lamp irradiation for 2 hours produces copper nanoplates. KrF laser irradiation at a low power of 3 mJ/cm^2 also generates copper nanosheets, efficiently. Figure 1 displays the change of the TEM images of the film as functions of irradiated number of laser pulses, 120 shots (a), 1200 shots (b) and 9600 shots(c). In Figure 1-a, one can see the formation of nuclei of metallic particles. The wavy lattice patterns with 0.3 nm spacing are thought due to the alignment of the original cluster molecules and the disorder can be produced by the formation of metallic nuclei. Further irradiation causes planer crystals as seen in (b). The spacing of the lattice pattern is regular and the interval is 0.26 nm. At this stage, the crystals exhibit grain boundaries with several 10 nm scales. In the planes dominated with metallic plates, one can find whity matrix rooms composed of segregated ($t$butyl-ethynyl)$_n$ polymers. However, further photon impact fills these spaces with joining metallic particles or plates nearby located on the lower side and made them into larger crystalline sheets as seen in Figure 1-c, where not only the (111) plane but also the (110) plane of copper fcc crystals are seen with a lattice spacing of 0.26 and 0.36 nm, respectively.

In Figure1-d, we show schematic explanation of the evolution of small particles to a nanosheet in the photon field. The observed phenomenon can be explained by plasmon–plasmon interaction induced by the photon electromagnetic field and surface enhanced photochemical reactions of the residual ethynyl copper cluster molecules that may also supply heat for rearrangement of metal atoms in the joining particles or sheets. Energy supply to metallic particles from light harvesting organic matrices can be also important to increase the internal

temperature of the metals.

Figure 1-e displays a cross-sectional view of the film deposited on a polyimide film after the irradiation of KrF laser pulses (12000 shots). Photolithographic dot patterning observed by a SEM is shown in Figure 1-f that was made with a chromium photo-mask and washing the residual cluster molecules by hexane. Each dot is spaced at every 1 μm. The surface is covered with the polymer layer thinner than 50 nm that is easily removed by laser sputtering.

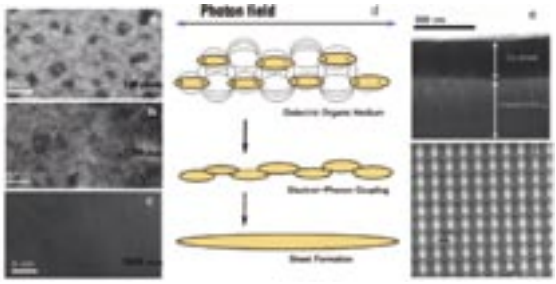

Figure 1. High resolution TEM images of the film as functions of irradiated number of laser pulses, 120 shots (a), 1200 shots (b) and 9600 shots(c). Laser energy density was 3 mJ/cm^2. (d) is schematic explanation of the evolution of small particles to a nanosheet in the photon field. (e) is a cross-sectional view of the film deposited on a polyimide film after the irradiation of KrF laser pulses (12000 shots). (f) is photolithographic copper-dot patterning obtained with a chromium photo-mask and washing the residual cluster molecules by hexane. Since, the copper surface is covered by thin polymer layer, copper parts look white.

III-A-4 Synthesis of Carbon-Encapsulated Nanoparticles *via* Thermal Decomposition of Metal Acetylide

NISHIJO, Junichi; OKABE, Chie; OISHI, Osamu; NISHI, Nobuyuki

[*Carbon* in press]

Carbon-encapsulated metal nanoparticles are promising materials for application in magnetic storage and battery due to their chemical stabilities. Though there are several methods of synthesizing the carbon-encapsulated nanoparticles such as arc discharge and thermal decomposition of hydrocarbons, the methods are not suitable for size-selective synthesis or mass production. Furthermore, the methods require a high temperature treatment which makes it difficult to synthesize carbon-encapsulated nanoparticles of metastable phases and low melting point metals. To solve these problems, we developed a new synthesis method for the carbon-encapsulated nanoparticles, where the carbon-encapsulated materials are formed by the low temperature thermal decomposition of the metal acetylide.

The acetonitrile suspension of metal chloride MCl_2 and calcium carbide CaC_2 sealed into the airtight vessel is heated to 240 °C for 12 h. In the solution, CaC_2 is gradually dissolved, and C_2^{2-} and M^{2+} form nanosized ionic cluster $(M^{2+}C_2^{2-})_n$ in the solution. Owing to the strong reducibility of C_2^{2-}, the cluster is converted into neutral metal-carbon cluster $(M^0C_2^0)_n$ by thermal energy. This neutral cluster is unstable because it can be regarded as metal-carbon supersatulated solid solution. As a result, metal atoms exclude the excess carbons and form carbon-encapsulated carbon-saturated metal nanoparticles. Figures 1 show the TEM images of carbon-encapsulated metal nanoparticles (M@C) of Sn, Pd, Ni and Co. As shown in the figures, each particle is covered with a carbon shell with the thickness of 2–6 nm which protects the metal or metal carbide core from the oxidation even in 1 M HClaq. The average core sizes depend on the metals; that is, 25, 8, 14 and 15 nm for M = Sn, Pd, Ni and Co, respectively.

The XRD patterns reveal the peculiar structures of the metallic cores. The core of Sn@C is pure metallic β-Sn, which reflects the instability of tin-carbide. On the other hand, other three metals prefer the carbide phases to metallic phases. The XRD pattern of Pd@C is explained as the sum of usual *fcc* and unusual *hcp* palladium carbide phases which has not been reported. In the case of M = Ni, Ni_3C phase is formed selectively. In contrast to the crystalline core structures mentioned above, the core of Co@C is almost all amorphous cobalt-carbon solid solution.

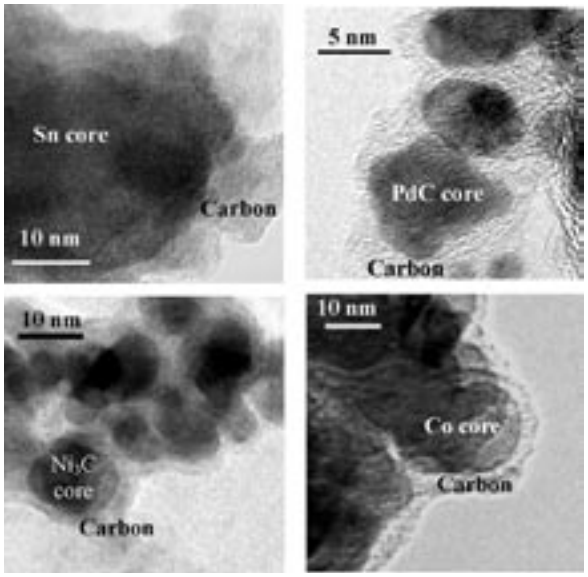

Figure 1. TEM images of carbon-encapsulated metal/metal carbide nanoparticles synthesized by thermal decomposition of metal-acetylide.

III-A-5 Synthesis, Structure and Magnetic Properties of a New Low-Spin Iron(III) Complex $[FeL_3]$ {L = $[HNC(CH_3)]_2C(CN)$}

NISHIJO, Junichi; NISHI, Nobuyuki

[*Eur. J. Inorg. Chem.* 3022–3027 (2006)]

High temperature treatment of acetonitrile with CaC_2 and $FeCl_2$ affords the new iron (III) S = 1/2 low-spin complex $[FeL_3]$ (L = $[HN{=}C(CH_3)]_2C(CN)$). The crystal structure and the inter-molecular overlap mode are largely affected by the crystal solvent ROH (R = Me, Et). In the $[FeL_3]$MeOH crystal, each MeOH molecule attracts $[FeL_3]$ complexes and disturb ligand–ligand interaction, resulting in the small overlap between adja-

cent complexes. On the contrary, [FeL_3] complexes form one-dimensional tunnel structure filled with EtOH molecules, where the inter-complex overlap is much larger as shown in Figure 1. The difference between the overlaps affects the inter-complex spin–spin interaction. The small overlap of [FeL_3]MeOH brings the negligibly small interaction, resulting in the Curie-like behavior of the spin. On the other hand, [FeL_3]EtOH behaves as singlet-triplet spin system with the interaction $2J/k_B$ = –7.5 K caused by stronger spin-spin interaction between adjacent complexes, which is originated from the large overlap between the π-electrons of the ligands. The EtOH crystal solvent can be easily removed only by evaporation owing to the tunnel structure of [FeL_3]EtOH, where the inter-complex interaction is reduced to negligibly small.

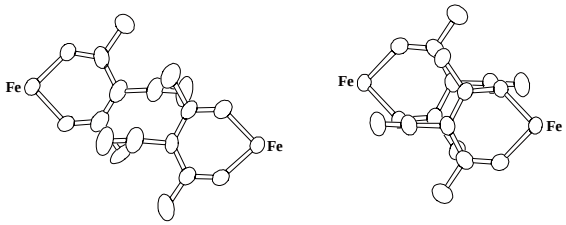

Figure 1. The inter-complex overlap mode of [FeL_3]MeOH (left) and [FeL_3]EtOH (right).

III-A-6 Preparation and Characterization of Gold Nanoparticles with Reactive Thiocarbonyls: A Proposal for Active Size Control of Nanoparticles

HINO, Kazuyuki[1]; NAKANO, Hirofumi[1],; ITO, Naomi[1]; MATSUSHITA, Machiko[1]; TAKAGI, Hideyuki[1]; NISHI, Nobuyuki
([1]Aichi Univ. Educ.)

[*Trans. Mater. Res. Soc. Jpn.* **31**, 525–528 (2006)]

Gold nanoparticles are prepared by using methyl-substitute 1,3-oxathiole-2-thione as a stabilizing reagent in the hydride reduction of tetrachloroaurate(III)ions. UV-vis absorption spectra and electron microscope observation show that the particle size can be controlled in a wide range from subnanometer to nanometer scale. Comparison of the results for these particles with those formed using methyl-substituted 1,2,4-trithiolane leads us to attribute the initial process of the formation of subnanometer-sized particles to the dimerization of 1,3-oxathiole-2-thione derivatives. In the reaction process, nascent particle surface is passivated with dimerization intermediates and the particle growth is terminated by sulfide formation.

III-B Ultrafast Dynamics and Scanning Tunneling Microscopy

Proton transfer and geometrical isomerization processes in electronic excited states are investigated with our pico-femto dual wavelength valuable systems. For the study of molecules on metallic or crystalline surface, very low temperature Scanning Tunneling Microscope (LT STM) system are now in use for collaboration with users in universities

III-B-1 Ultrafast Dynamics of Excited States of Chromium(III) Porphyrin Complexes in Solution

INAMO, Masahiko[1]; OKABE, Chie; NAKABAYASHI, Takakazu[2]; HOSHINO, Mikio[3]; NISHI, Nobuyuki
([1]Aichi Univ. Educ.; [2]Hokkaido Univ.; [3]RIKEN)

Cr(III) porphyrin complexes show variety of chemical reactivity and photophysical processes in their electronic excited states. In the present study, relaxation dynamics of the excited states following the Soret band excitation of the Cr(III) tetraphenylporphyrin complexes, [Cr(TPP)(Cl)(L)] (L = H_2O, Py, 1-MeIm), has been investigated using femtosecond time-resolved absorption spectroscopy in the toluene solution. The dynamics of the decay of the transient absorption spectra measured within a time domain of 400 ps is discussed with the various physical and chemical processes. In the case of [Cr(TPP)(Cl)(H_2O)], the biexponential decay of the initially populated excited state was observed with rate constants of $k_1 = 6.8 \times 10^{10}$ s^{-1} and $k_2 = 1.6 \times 10^9$ s^{-1}. These processes were assigned to the photodissociation of a H_2O ligand in the $^4S_1$ excited sate followed by the energy dissipation to electronically ground state [Cr(TPP)(Cl)]. On the contrary, the 1-MeIm complex [Cr(TPP)(Cl)(1-MeIm)], in which only the triplet excited state was observed using nanosecond transient spectra, shows a single exponential decay of the excited state. This was assigned to the decay of $^4S_1$ to T_1 with a rate constant of 3.8×10^9 s^{-1}. The excitation to S_2, the Soret band, occurs for 395 nm excitation followed by the intramolecular process of electronic, vibrational, and singlet-triplet relaxation with time scales of subfemtosecond, subpicosecond, and nanosecond, respectively, for a free base porphyrin. These findings indicate that the initially observed excited states in the present study may be $^4S_1$, and the S_2 to S_1 relaxation may be too fast to be observed in the present measurement. The lifetime of the $^4S_1$ excited states of [Cr(TPP)(Cl)(1-MeIm)] is much shorter than those of the porphyrin species that produce no paramagnetic ion due to the presence of the Cr(III) ion, but substantially longer than those of paramagnetic complexes such as [Cu(TPP)].

III-B-2 Scanning-Tunneling Microscopy, Near-Edge X-Ray-Absorption Fine Structure, and Density-Functional Theory Studies of N_2O Orientation on Pd(110)

WATANABE, Kazuo[1]; KOKALJ, Anton[2]; HORINO, Hideyuki[3]; RZEZNICKA, Izabela I.[2]; TAKAHASHI, Kazutoshi[3]; NISHI, Nobuyuki; MATSUSHIMA, Tatsuo[3]
([1]Fritz-Haber-Inst Max-Planck-Gesellschaft; [2]J. Stefan Inst.; [3]Hokkaido Univ.)

[*Jpn. J. Appl. Phys.* **45**, 2290–2294 (2006)]

The orientation of adsorbed N_2O on Pd(110) was studied by scanning tunneling microscopy, near-edge X-ray absorption fine structure (NEXAFS), and density functional theory. Below 14 K, N_2O(a) forms clusters extending along the $[1\bar{1}0]$ direction as well as monomers oriented along the [001] direction. In the clusters, N_2O is tilted with the terminal nitrogen bonding to the surface. The clusters are mobile at 14 K and stable at 8 K, whereas the monomers are stable at 14 K. In NEXAFS work at 60 K, remarkable anisotropy was found in the polarization dependence of π resonance, which was consistent with a mixture of the tilted and [001]-oriented forms.

III-C Spectroscopic and Dynamical Studies of Molecular Cluster Ions

Electron defficiency of molecular cluster cations can attract electron rich groups or atoms exhibiting charge transfer or charge resonance interaction in the clusters. This causes dynamical structural change such as proton transfer or ion-core switching in hot cluster ions or clusters in solution.

III-C-1 IR Photodissociation Spectroscopy of Hydrated Noble Metal Ions: Coordination and Solvation Structures

IINO, Takuro[1]; INOUE, Kazuya[1]; OHASHI, Kazuhiko[1]; MUNE, Yutaka[1]; INOKUCHI, Yoshiya[2]; JUDAI, Ken; NISHI, Nobuyuki; SEKIYA, Hiroshi[1]
([1]Kyushu Univ.; [2]Hiroshima Univ.)

Hydrated noble metal ions, $M^+(H_2O)_n$ (M = Cu, Ag), are studied by infrared photodissociation spectroscopy and density functional theory calculations. The third water in $Cu^+(H_2O)_3$ is hydrogen-bonded to one of the two waters coordinated to Cu^+, while all waters in $Ag^+(H_2O)_3$ are directly bonded to Ag^+. The difference in the coordination number is attributable to the different degree of *s-d* hybridization between Cu^+ and Ag^+.